An improvement of heterogeneous catalyst Fe3O4@MnO2 nanocatalyst on bio-diesel production from castor oil

SAKTHI SARAVANAN (mohans@vicas.org)
Nandha Engineering College
Periyasamy Sivanandi
Government College of Technology

Research Article

Keywords: castor oil, Fe3O4@MnO2, methanol, AFM, XRD

Posted Date: June 1st, 2022

DOI: https://doi.org/10.21203/rs.3.rs-1620062/v1

Abstract

The exhaustion of natural resources has occasioned the profit margin of oil products to increase dramatically, prompting the use of sustainable fuels like as biofuel. In the proposed investigation, biofuel was developed from castor oil utilizing Fe_3O_4@MnO_2 NCs as a heterogeneous catalyst for the transesterification process. X-Ray Diffraction evaluation acknowledged the nanocatalyst's single phase. Scanning Electron Microscopy revealed the spherical morphology of the consolidated nanocatalyst. The magnetic characteristics were examined using a vibrating sample magnetometer. Atomic Force Microscopy demonstrated that the catalyst exhibited has a greater surface area and unevenness. The yield was achieved was 95 percent (w/w) in 50 minutes at 60^0 C with 15 wt percent catalyst loading and a 12:1 methanol/oil ratio, as acknowledged by a gas chromatograph with mass spectrometer. The findings indicate that Fe_3O_4@MnO_2 NCs are an encouraging catalyst for bio-fuels production via heterogeneous catalyzed transesterification under relatively mild response circumstances.

1. Introduction

The massive global scramble against options available to petroleum product offerings to counteract ecological issues had also received a lot of attention awhile back. From 2016 to 2020, the global biofuel industry is projected to grow by 14% in terms of driving climate adaptation and mitigation. The expected bio-fuel constraint in 2020 is 33.2 billion liters, which is noticeably greater than the upper in 2016 [1]. Glycerol or glycerin is a substantial adventure mode in the biofuel production process. It's also been encountered that glycerine is presented with methanol as an undesirable hand in the preparatory work of unsaturated lipid transesterification process. Besides that, except in the manufacturing of 100 pounds of bio-fuel, nearly 10 pounds of jagged glycerol are presented [2]. As a necessary consequence, bio-fuel production may lead to the enhancement of crucial synthetic drugs in food, drug, and beauty and cosmetic item expeditions.

Biofuels is primarily developed through the transesterification of scrap cabbage oil, green algae oil, or peanut oil as a raw material. It is a response that occurs among triglyceride levels and alcohol in the existence of an appropriate catalyst to produce FAME and glycerin. Bioethanol or ethyl alcohol is by far the most frequently utilized alcohol [3]. Castor is one of the seedlings with the highest oil harvest prospects due to its high seed produce and sulfur content in its seedlings. Castor oil is a rich source dynamic viscosity due to its high subject matter of ricinoleic acid, which has a hydroxyl group. They are also distinguished by their good stabilization and hydrophilicity. The propensity of almond oil to dissolve in alcohol influences the biodiesel production operation [4].

Several investigations have been performed to profile for biofuel production terms of essential or acidic motivations utilizing effective approach [5, 6]. But now day’s Magnetic nanomaterials are found to be more selective and effective than conventional heterogeneous materials as a robust, readily available, extremely small size and large surface area of heterogeneous catalyst support. Further, it has more volume ratio which allows more reactions to occur at the same time and consequently speed up the

reaction process [7–8]. Advantageously, they are magnetically separable, which eliminates the requirement of catalyst filteration or centrifugation after completion of the reaction. The Fe3O4 MNPs, due to their unique physicochemical properties becoming increasingly significant in the field of catalysis, imaging, photonics, nanoelectronics, sensors, biomaterials, and biomedicine [9].

Henceforth, the recent finding expected to focus on utilizing castor oil as a biofuel origin to use an Fe_3O_4@MnO_2 nanocatalyst by tuning the parameters such as adsorbent dose, oil:methanol ratio, reaction temperature, and reaction time. The kinetic models of the transesterification method were also explored, and the biofuel obtained was categorized in order to achieve full their great promise.

2. Materials And Methods

2.1 Required materials

Essential oil has been used to perform out the transesterification process. Chemicals required for the synthesis of catalyst and production of biodiesel are Ferric chloride, ferrous sulphate, manganese sulphate, Sodium Hydroxide, polyethylene glycol and Methanol were acquired from Chemspure, Chennai, Reachem chemicals, Chennai, and Merck, India, subsequently.

2.2 Magnet preparation

Fe_3O_4 nanoparticles were established using a simplistic co-precipitation strategy, as described in the following: 2mol/L NaOH administrations and a 5 percent polyethylene glycol (Stake) design have been suitable for immediate use. Extracted were 100 mL of deionized water, 3.24 g of $FeCl_3$, and 2.39 g of $FeCl_2$•$4H_2O$. Following that, we combined FeCl3, $FeCl_2$•$4H_2O$, and 5% PEG for 10 minutes with ultra - sonic movement [10]. The slurry has been kept to 75°C, and then 2 mol/L NaOH was introduced till the pH of the blends was around 11.5. Incorporating and blending occurred at 60°C for two hours, followed by 30 minutes of improvement at 80°C. The nanoparticles were then sterilized on a routine basis utilizing applied magnetic field detachment, managed to wipe countless times with ultra - pure water or ethanol, and dried at 80°C.

2.3 Synthesis of core magnet catalyst (Fe_3O_4/MnO_2 NCs)

A Fe_3O_4/MnO_2 nanocomposite with a core magnetic was designed and built in a continuous cycle. The term "precipitation methodology" refers to a method for forecasting the proportion of rain that will drop. 0.5 g Fe_3O_4 particles were scattered in 100mL 5 percent Stake for 30 minutes by ultra - sonic swirling, then incorporated in with 100mL $MnSO_4$ grouping of exact immobilization, supported by additions of NH_3•H_2O formation in a typical mixing. The impact lasted for 12 hours at 60 degrees Celsius. During the conclusion of the period, the aggregates were extracted and washed countless times with purified water utilizing aesthetically effective barriers [11]

2.4 Bio-diesel production method

Transesterification of castor oil was carried in batch process in a 500 ml beaker using magnetic stirrer and heat plate arrangement. The process was carried by mixing desired amount of catalyst with required amount of methanol. Then the oil was added to the mixture containing the catalyst and methanol in beaker. Quantity of catalyst to be measured depends upon the oil g/g oil. The requisite temperature was maintained and the set up were left undisturbed depending upon the reaction time required. After the desired duration, the mixture was transferred to the separating funnel for the separation of the desired product. The set up were again left undisturbed for 2 h for the separation of lighter phase and darker phase. Glycerol obtained at the bottom was withdrawn. The obtained biodiesel was washed and measured. The bottom catalyst layer was removed carefully and regenerated. The regenerated catalyst was successively used to study the reusability. Transesterification reactions were carried by varying catalyst concentration, O/M ratio, reaction time, temperature about 2–18%, 1:5 – 1:14, 10–60 min and 40-80^{0}C respectively. The biodiesel produced consists of methyl esters, monoglycerides, diglycerides, and unreacted triglycerides and they were characterized by Gas Chromatography along with Mass Spectrometry and the yield or conversion was calculated.[12]

2.5 Kinetic studies

The experiment was carried out at different temperatures at 40, 50, 60, 70 and 80^0 C and tested for order of kinetics of the reaction. The kinetics of the transesterification reaction is represented by Eq. (1).

$d[P]/d[t] = k[P]$----------(1)

Where P is methyl esters in terms of yield (%), t is the reaction time (min), and k is rate of the reaction (min1). The ln[P] versus ln[dP]/dt at different interval of time and temperature were plotted. The rate constant was determined from intercept and slope. Arrhenius equation in Eq. (2) was used to study the influence of temperature on the specific reaction rate.

$k = Ae^{-(Ea/RT)}$ ---------- (2)

where " Ea" is the activation energy (J/mol), define as the minimum energy required to start a chemical reaction, R is the gas constant (8.314 J/mol.K), T is the absolute temperature (K), A is the frequency factor (collision factor) and k is the reaction rate constant. The slope and intercept of the graph between ln k versus 1/T give the values of activation energy [13].

3. Results And Discussion

3.1 Crystallite phase investigation

[Figure-2] illustrates the X-ray obstruction framework of the two specimens that emerged before it. Whereas relatively limited template represents frequent Fe_3O_4 fragments, the existence of MnO_2 in the Fe_3O_4/MnO_2 lattice is recommended by comparative recognisable peaks at 2θ = 27.5 and 2θ = 40.3 in the located in the outer line. This it seems to be due to the influence of the sharp phases. As stated

previously, the crystallographic peaks were detected to be mainly correlated to the magnetite cubical symmetric spinel platform's standard template recognisable peak position (JCPDS 01-072-2345). Using the Scherrer equation, we assessed the crystalline structure of Ferrite nanoparticles and acquired 19.64 nm [14].

3.2 FT IR analysis

[Figure-3] depicts the FTIR spectrum of Fe_3O_4/MnO_2 nanocomposite. The recognizable peak observed of Fe_3O_4/MnO_2 composite particles is located at 647 cm^{-1}. It's possible that the Fe-O-Mn particles were bind to the monodispersive compared to the feedstock oil. It is noteworthy that a novel peak at 439 cm^{-1} originated in the ability to respond of the nanocomposites, suggesting that a new bond was formed between both the core and the shell. The absorption peaks near 3711.9 and 3157 cm^{-1} are adaptable oscillating hydroxy peaks on the surface of substrate; they are broader and powerful than that of the Fe_3O_4 absorption bands. It assumes that the composite particles encompass more hydroxys than Fe_3O_4, which may increase the activity of MnO_2 particles [15].

3.3 Morphological investigation

[Fig-4 (a)] shows the structural and morphological spectrum of $Fe_3O_4@MnO_2$ NCs. These SEM images showed granular shapes with no assemblage and un equality of homogeneously $Fe_3O_4@MnO_2$ NCs. Figures 4 (c) HRTEM shows the surface characteristics of $Fe_3O_4@MnO_2$ NCs. [Fig-4 (b)] shows that TEM images of $Fe_3O_4@MnO_2$ NCs indicate rod like spherical in patterns with molecule size varying from 12 to 22 nm. Furthermore, the monocrystalline phase of $Fe_3O_4@MnO_2$ NCs by co-precipitation strategy was supported by their corresponding SAED examination, as shown in Fig. 4 (d), with recognizable peak (311), (400), (422), (511) and (400) crystallographic patterns recommending cubical symmetric spinel strategy. The HR-TEM illustration also reveals a well inner surface of the ligament, with the d –widths for adjoining interlayer fringes one assessed to be 0.236 nm, that also represents the proportion of the (311) plane cubical symmetric spinel of $Fe_3O_4@MnO_2$ NCs [16, 14]

3.4 BET isotherm of $Fe_3O_4@MnO_2$NCs

The N_2 adsorption-desorption isotherm models and pore size diffusion of a novel $Fe_3O_4@MnO_2$ impetus are displayed in Fig. 5 (a & b). Figure 5 (a) illustrates an impressively genuine $MnO_2@Fe_3O_4$ impetus with a group IV isotherm, which emerges to be a characteristic revealed by hierarchical highly permeable components. The inter - facial state (SBET) was assessed using Brunauer–Emmett–Teller (BET) approach, and the pore diameter correspondence was acquired utilising the Barrett–Joyner–Halenda (BJH) tactic case and even the adsorption isotherm band. Figure 5 (b) demonstrates how the volume immobilized rapidly with increasing comparative imperative attributes for all isotherms depending on the volume required to fill of mesopores in Fe_3O_4 screenplay. The porosity and surface province of $MnO_2@Fe_3O_4$ and the permeability length across were characterised to be 13.19 m^2/g and 0.059 cm^3/g, respectively [17]

3.5 EDX spectrum and Elemental mapping Analysis

Elemental analysis of Fe_3O_4@MnO_2 NCs photo detectors demonstrated that certain components, chiefly iron, oxygen, and Mn were generally provided in the hybrid Fe3O4@MnO2 nanocomposite. Moreover, the EDX template of Fe_3O_4@MnO_2 NCs reported the existence of all component parts including such Fe, O, and Mn were shown in Fig – 6 [18]

3.6 AFM analysis

The AFM is a type of electron microscopy that is being used to detect factors like length. In tapping phase, an AFM image of Fe_3O_4/MnO_2 was captured. Surface morphology, which is commonly expressed in dimensions of exterior hardness, is essential for forecasting catalytic characteristics. The root mean square roughness (RMS) of a material is related to its particle diameter. The average rough surface was 5.89 nm, with the Root Mean Square at 10.37 nm. The rougher the texture and the greater the contact area, the more activation centres there are. The excessive annealing temperature [19] may have caused the nanocatalyst's irregular structure.

3.7 Magnetic behavior of synthesized Fe_3O_4/MnO_2 nanocomposites

The magnetic profiles of Fe_3O_4 nanoparticles and Fe_3O_4/MnO_2 omposite fragments are shown in Fig. 7(a) and (b). Two very different designs are similar, and the Fe_3O_4/MnO_2 composite particles possess super-paramagnetic characteristics. Even as permanent magnet field was curtailed, the ferromagnetism lessened until it dropped to zero at H = 0. No residual magnetic moment stayed. It further inhibits particle aggregation, and the powders could be incredibly quickly distributed equally because once the magnetic field is excised. Fe3O4 nanoparticles have a saturation magnetization of 68.1 emu/g, while Fe3O4/MnO2 considered as part have a magnetization of 33.5 emu/g.[14, 20]

3.8 Effect of core magnet Fe_3O_4/MnO_2 catalyst loading on biodiesel production

Effect of Fe_3O_4/MnO_2 nanocomposites posses basic surface sites, which make them highly efficient in catalytic processes. Transesterification reaction was strongly affected by catalyst concentration. Biodiesel conversion was investigated with 12:1 M ratio of methanol: oil at a temperature of 55^0C for 50 min. When the catalyst concentration was increased from 5wt % to 15wt% the conversion was increased from 4–90% respectively as shown in Fig. 9 (a). However when the catalyst concentration was increased beyond 15 wt%, there is slight reduction in the conversion due to slurry being viscous and emulsified [21]

3.9. Effect of methanol to oil ratio on biodiesel production

Important factor governing the biodiesel conversion is methanol to oil molar ratio. The stoichiometry ratio of the transesterification reaction requires 3 mol of methanol to yield 1 mol of glycerol and 3 mol of fatty esters. Being a reversible reaction excess methanol is used to shift the reaction to the right. The reaction

was carried out by varying molar ratios of methanol from 5:1 to 14:1 under the conditions of 14 wt% catalyst, reaction temperature of 60^0 C in 50 min. Conversion of biodiesel was increased from 9 to 90% as the molar ratio increased from 5:1 to 12:1 (Fig. 9 (b)). The conversion decreased from 90–78% when the molar ratio was further increased from 12:1 to 14:1, this is due to accumulation of methanol and viscous nature of the fluid [22].

3.10. Effect of temperature on biodiesel production

Reaction temperature is another important criterion that will affect the yield of biodiesel. Each experiment was run for 50 min with 15 wt% catalyst and 12:1 methanol oil molar ratio. The reaction temperature was varied from 40 to 80^0 C as shown in Fig. 10 (a). The result indicates that the biodiesel conversion was low at lower temperature with only 60% at 40^0 C, biodiesel conversion increased sharply and reached 95% at 60^0 C. Increase in the temperature increases the yield respectively due to increase in the solubility of the solvent with enhanced diffusion rate. The conversion dropped on further increase in temperature 88% at 70^0C. The yield tends to decrease after certain temperature due to methanol vaporization [23].

3.11. Effect of reusability of Fe_3O_4/MnO_2 NCs

Reusability is one of the most important features of a heterogeneous Fe_3O_4/MnO_2 catalyst. Catalysts were reused to test the lifetime and stability of the catalyst. The catalyst used after the first cycle was collected and dried for the use in the successive cycles. To study the effect of reusability, experiments were carried out at 60^0 C, with a 12:1 methanol to oil ratio, 14 wt.% of catalyst for 50 min. The activity of the regenerated catalyst used for the sequential steps tends to remain stable for four cycles where the yield was around 95% (Fig. 8). The conversion was 87% after fourth cycles and tends to decrease at faster rate due to the deactivated active sites [24]

3.12. Kinetic investigation

The kinetic survey was done by appropriate conditions for the transesterification process. The average rate variable at various heating rate (40–800 C) for the biodiesel synthesis of castor oil engendered by Fe_3O_4/MnO_2 NCs has been estimated Nanocatalyst. Transesterification reaction tends to follow the first order reaction as the product formations (Methyl esters) are studied as function of time. Plot of ln[p] versus ln(dp/dt) at different interval of time and temperature was found to be linear where rate constant was determined from intercept and slope. The yield tends to increase with respect to time and temperature where the reaction rate rises with increase in temperature [25]. Thus the reaction rate is dependent on reaction temperature and time. Arrhenius relationship and the activation energy were studied for the transesterification process. The activation energy (Ea) was calculated using Eq. (3).

$$\ln k = - Ea/RT + C \quad \text{——————} \quad (3)$$

The activation energy was calculated from the slope of 1/T versus (ln k). The first order tends to fit the kinetic model. The activation energy required for transesterification of castor oil catalyzed by

nanocatalyst was found to be 1627.23 J/mol.

3.14 Bio-fuel assessment

The fatty acid methyl ester contents of biofuels compounds were characterized employing Gas chromatography - mass in detection mode, as demonstrated by earlier work. The prevalence of methyl esters is indicated by the distinct peaks in Fig. 11. The greatest signal, with latency duration of 18.7 minutes, shows the existence of 9-octa decenoic acid, methyl ester [26].

4. Conclusion

Fe_3O_4 and Fe_3O_4/MnO_2 nanocomposites constructed by co-precipitation integral approach. Catalytic performance for the biodiesel production of essential oil (castor oil) utilizing methanol. All of the specifications explored, including response time, catalyst dosage, heating rate, time, and methanol to oil molar ratio, had a massive implication on the heterogeneous transesterification of Castor oil. At perfect circumstances, the cumulative extraction yields from Castor oil was 95%: 50 minutes of response time, 60^0C temperature, 15 wt% catalyst dosage, and a methanol to oil molar ratio of 12:1. The first order tends to fit the kinetic model, with an activation vitality of 1627.23 J/mol. Finally the Fe_3O_4/MnO_2 core shell magnet was very effective nature in biofuel production from castor oil.

Declarations

Author acknowledgement; Authors are thanks to my research Supervisor and providing facility for our research work, department of Mechanical Engineering, Government College of technology, Coimbatore-641013, TN-India, and extend thanks to instrumentation facility providing PSG-College of Technology, Coimbatore.

Author information; Department of Mechanical Engineering, Government College of technology, Coimbatore-641013, TN-India,

Sakthisaravanan & periyasamysivanandi

Department of Biotechnology, Vivekananda College of Engineering for women (Autonomous), Tiruchengode, Namakkal-637205, TN-India

M.S Manojkumar

Corresponding Author; correspondence to astromoha88@gmail.com, speriyyasamy@gmail.com

Ethics declaration; Ethics is not applicable

Consent to participate; None

Consent for publication; not applicable

Competing interest; the authors declared there is no competing interest

References

1. Hajjari M, Tabatabaei M, Aghbashlo M, Ghanavati H (2017) A review on the prospects of sustainable biodiesel production: a global scenario with an emphasis on waste-oil biodiesel utilization. Renew Sustain Energy Rev 72:445e464
2. McGinnis L (2007) Fueling America-without petroleum. Agric Res 55(4):10e13
3. Krawczyk T (1996) Biodiesel- alternative fuel makes inroads. but hurdles remains Inform 7:801e829
4. Theam KL, Islam A, Choo YM, Taufiq-Yap YH (2015) Biodiesel from low cost palm stearin using metal doped methoxide solid catalyst. Ind Crop Prod 76:281e289
5. Islam M, Ahmed AS, Islam A, Abdul Aziz S, Xian LC, Mridha M (2014) Study on emission and performance of diesel engine using castor biodiesel.J. Chem.1e8
6. Montazeri H, Amani A, Shahverdi HR, Haratifar E, Shahverdi AR (2013) Design and development of a novel magnetic camphor nanospheres core/shell nanostructure. J Nanostruct Chem 3:25–31
7. Nasir Baig RB, Rajender SV (2013) *Chem. Commun.*, A facile one-pot synthesis of ruthenium hydroxide nanoparticles on magnetic silica: aqueous hydration of nitriles to amides, J.Chem.communications *49*,752–770
8. Ricciardi R, Huskens J, Verboom W *ChemSusChem (***2015)**,Nanocatalysis in Flow*8*,2586–2605
9. Yin L, Liebscher J (2007) **()**, **Carbon** – **Carbon Coupling Reactions Catalyzed by Heterogeneous Palladium Catalysts** Chem. Rev. 107, **133**–**173**; (**b**) **Phan N**.**T**, Sluys M.V.D, Jones C.W, (**2006**) **Polyvinylpyridine**-**Supported Palladium Nanoparticles**: **An Efficient Catalyst for Suzuki**–**Miyaura Coupling Reactions** Adv. Synth. Catal. 348, **609**–**679**; (**c**) **M**. **Moreno**-**Manas**, **R**. **Pleixats**, **Formation of Carbon** – **Carbon Bonds under Catalysis by Transition**-**Metal Nanoparticles** Acc. Chem. Res. 36, **638**–**643**
10. Weia Y, Hanb B, Hua X, Linc Y, Wangd X, Denga (2012), Synthesis of Fe3O4 nanoparticles and their magnetic properties, Procedia Engineering 27, 632–637
11. Boopathy Gnanaprakasam AM, Pandey SG, Agalave, Vinod CP (2019) MnO2@Fe3O4 MNP: An Efficient and Recyclable Heterogeneous Catalyst for Benzylic sp3 C-H Oxidation, *Chem. Asian J.* 9, 1;14(19):3414–3423;DOI;10.1002/asia.201900810
12. Baskar G, Soumiya S (2016) Production of biodiesel from castor oil using iron (II) doped zinc oxide nanocatalyst. Renewable Energy 98:101–107
13. Freedman B, Butterfield RO, Pryde EH (1986) Transesterification kinetics of soyabean oil. J Am Oil Chem Soc 63:1375–1380
14. Zhang Shu and ShulinWang (2009) Synthesis and Characterization of Magnetic Nanosized Fe3O4/MnO2 Composite Particles Journal of Nanomaterials. Article ID 340217:5. doi:10.1155/2009/340217

15. Jafari L, Pourahmad A, Asadpour L (2017) Rice husk based MCM-41 nanoparticles loaded with Ag2S nanostructures by a green and room temperature method and its antimicrobial property. Inorg Nano Metal Chem 47:1552–1559
16. Boopathy Gnanaprakasam AM, Pandey SG, Agalave, Vinod CP (2019) MnO_2@Fe_3O_4 MNP: An Efficient and Recyclable Heterogeneous Catalyst for Benzylic sp3 C-H Oxidation, *Chem. Asian J.* 9, 1;14(19):3414–3423;DOI;10.1002/asia.201900810
17. Guo F, Li H, Zhang Z, Meng S, Li D (**200)9**, Synthesis of mesoporous YF_3 nanoflowers via solvent extraction route,Mater. Sci. Eng., B, 163,134–137
18. Anurag Kumar, Aathira MS, Pal U, Jain SL (2018) Photochemical Oxidative Coupling of 2-Naphthols using Hybrid rGO/MnO2 Nanocomposite under Visible Light, ChemCatChem. 10:1844–18528
19. Baskar G, Gurugulladevi A, Nishanthini T, Aiswarya R, Tamilarasan K ,(2017),.Optimization and kinetics of biodiesel production from mahua oil using manganese doped zinc oxide nanocatalyst.Renew. Energ.103,641–646
20. Teo SH, Islam A, Chan ES, Thomas Choong SY, Alharthi NH (2019) Yun Hin Taufiq-Yap, Md Rabiul Awual, Efficient biodiesel production from Jatropha curcus using $CaSO_4$/ Fe_2O3-SiO2 core-shell magnetic nanoparticles, Journal of Cleaner Production 208, 816–826
21. Wang X, Liu X, Zhao C, Ding Y, Xu P (2011) Biodiesel production in packed bed reactor using lipase nanoparticle biocomposite. Bioresour Technol 102:6352e6355
22. Meher LC, Vidya Sagar, Naik SN (2006) Technical aspects of biodiesel production by transesterification - a review, Renew. Sust Energy Rev 10:248–268
23. Rudzinski W (1997) A new theoretical approach to adsorption Desorption kinetics on energetically heterogeneous flat solid surfaces based on statistical rate theory of interfacial transport. Stud Surf Sci Catal 104:335–337
24. Pasupulety N, Gunda K, liu Y, Rempel L, T (2013) Flore, Production of biodiesel from soybean oil on CaO/Al2O3 solid base catalysts. Appl Catal A 452:189–202
25. Suganya T, Renganathan S (2012) Optimization and kinetic studies on algal oil extraction from macroalgae Ulva lactuca. Bioresour Technol 107:319–326
26. Baskar G*, Soumiya S (2016) Production of biodiesel from castor oil using iron (II) doped zinc oxide nanocatalyst. Renewable Energy 98:101–107

Figures

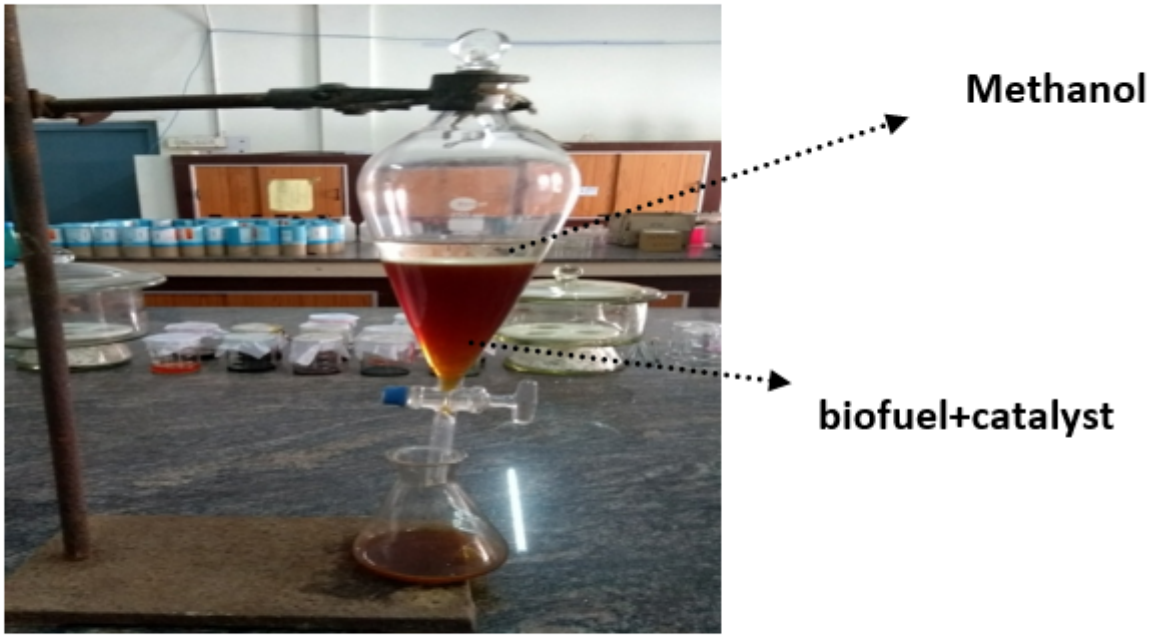

Figure 1

scheme representation of biofuel production using core magnet Fe_3O_4/MnO_2 NCs

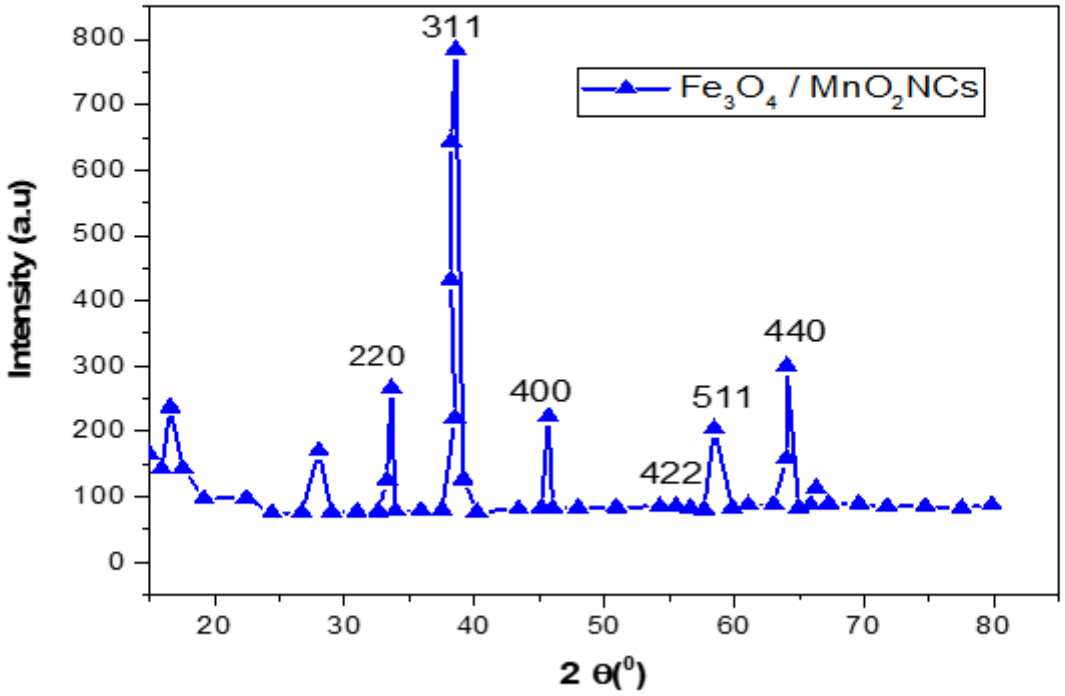

Figure 2

powder x-ray diffraction pattern of Fe_3O_4/MnO_2 nanocomposites

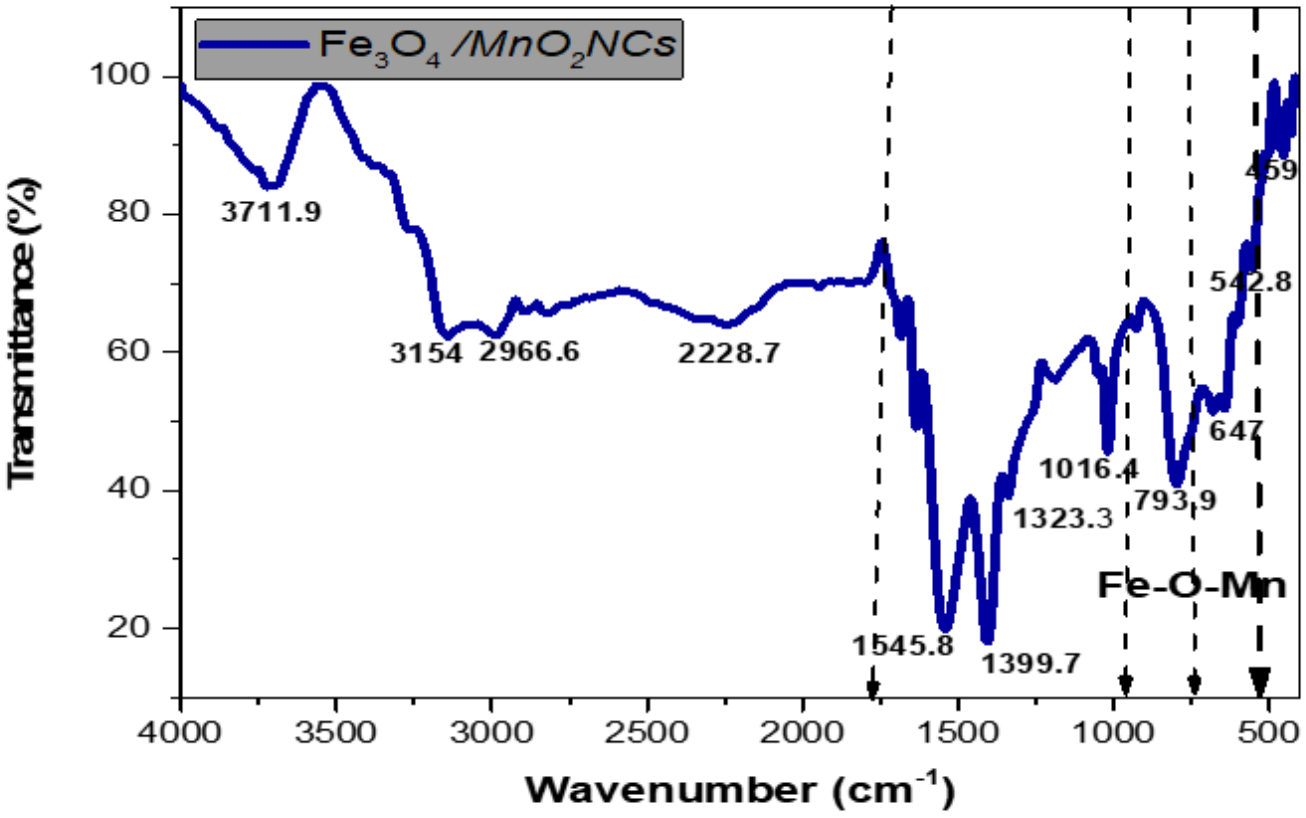

Figure 3

Functional group analysis of Fe_3O_4/MnO_2 NCs using co-precipitation method

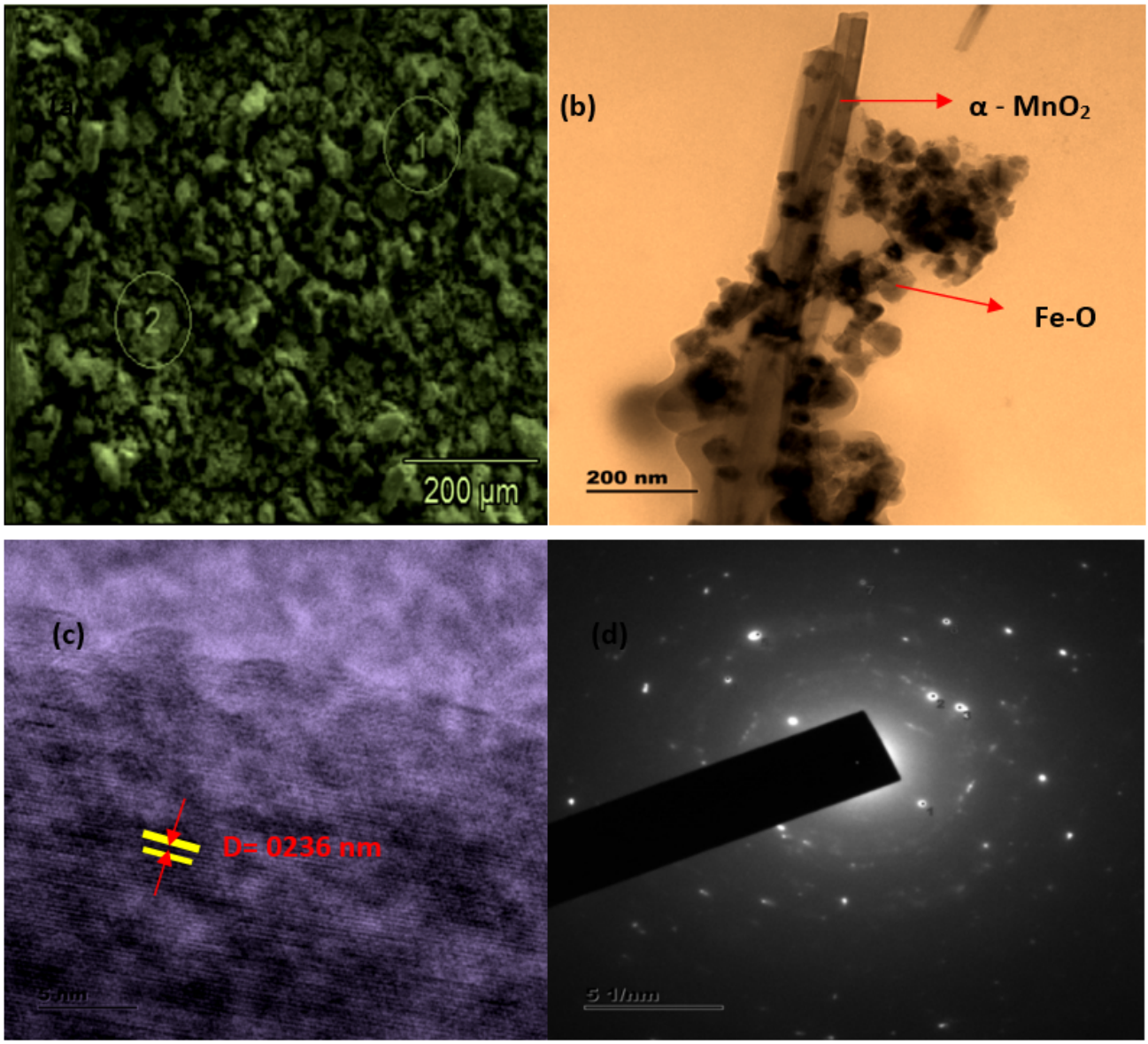

Figure 4

(a) SEM image of Fe_3O_4@MnO_2 (b) TEM microscopic spectrum of Fe_3O_4@MnO_2 NRs (c) HR-TEM image of Fe_3O_4@MnO_2 (d) SAED pattern of Fe_3O_4@MnO_2 NCs

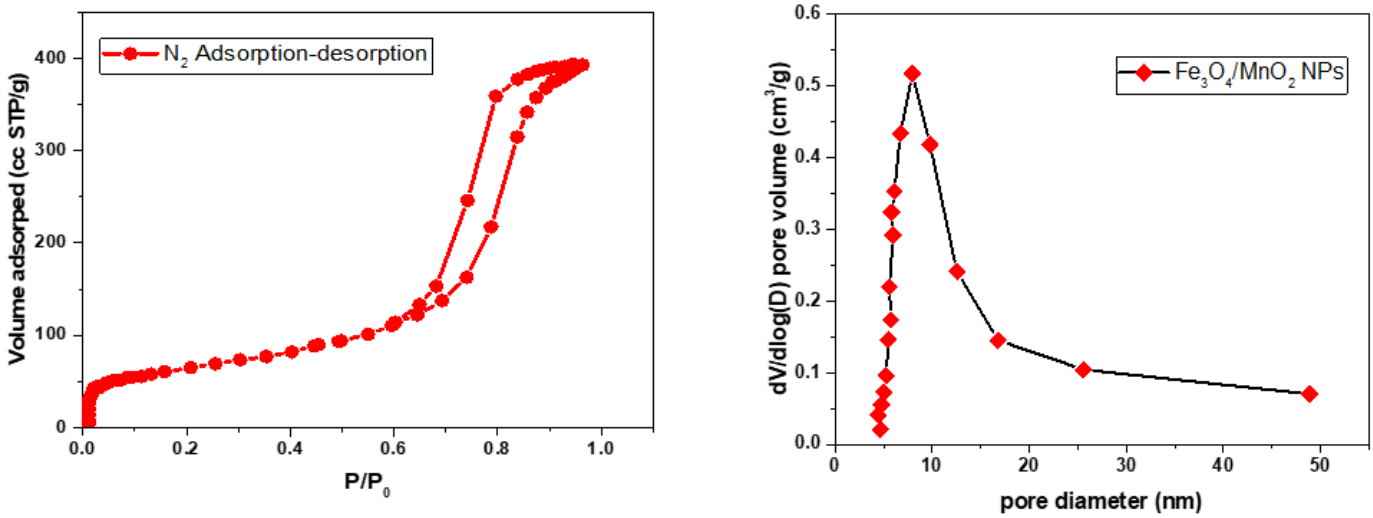

Figure 5

(a) N_2 adsorption-desorption isotherms (b) pore volume vs pore diameter of Fe_3O_4/MnO_2 NCs

Figure 6

(a) energy dispersive spectroscopy (b) elemental mapping spectrum

Figure 7

Atomic force microscopy of synthesized Fe_3O_4/MnO_2 NCs

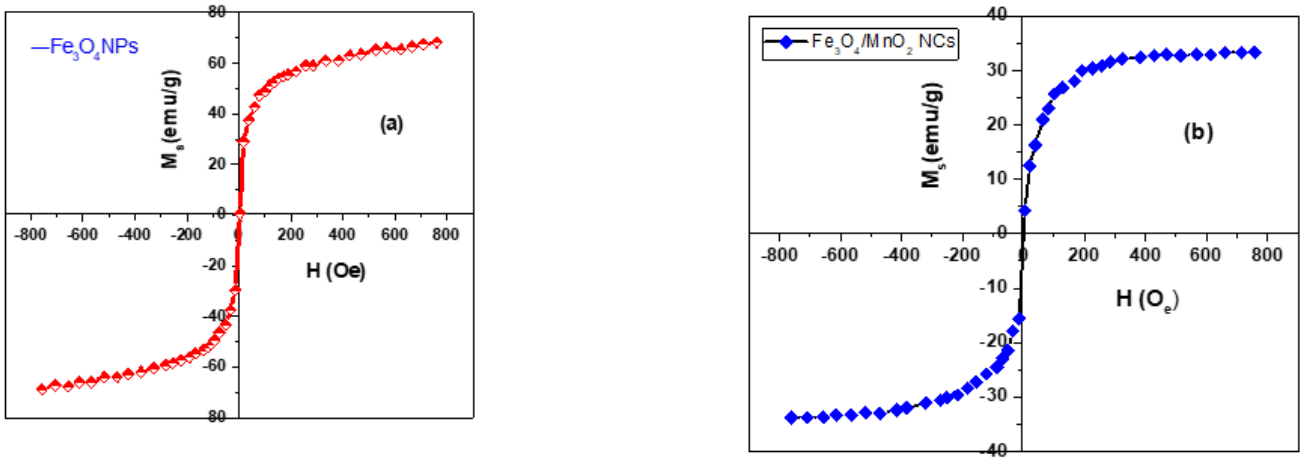

Figure 8

VSM spectra for (a) Fe_3O_4 (b) Fe_3O_4/MnO_2 nanocomposites by co-precipitation method

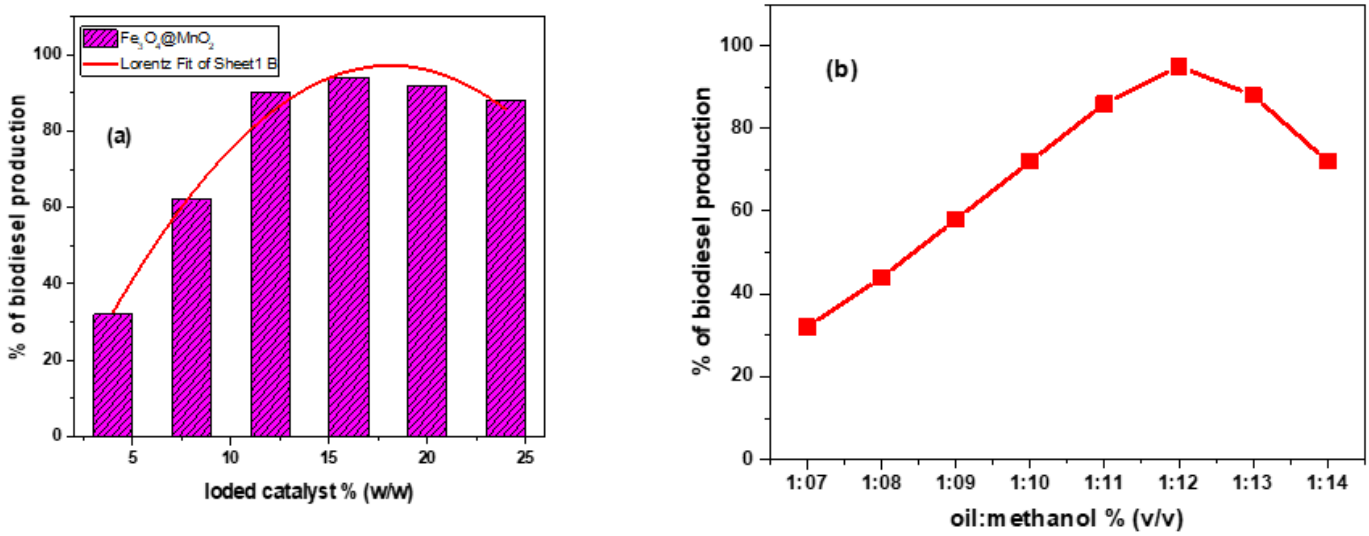

Figure 9

(a) effect of core magnet catalyst loaded (b) effect of methanol to oil ratio on biofuel production

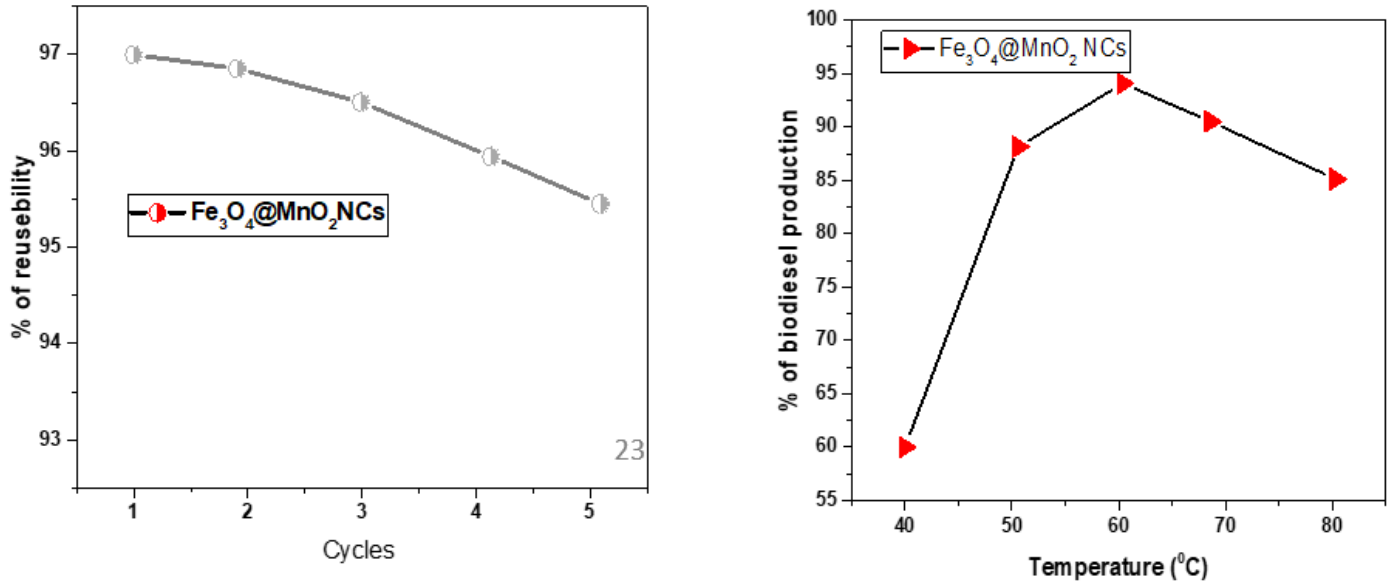

Figure 10

(a) reusability curve after five cycles (b) effect of temperature on biofuel production method

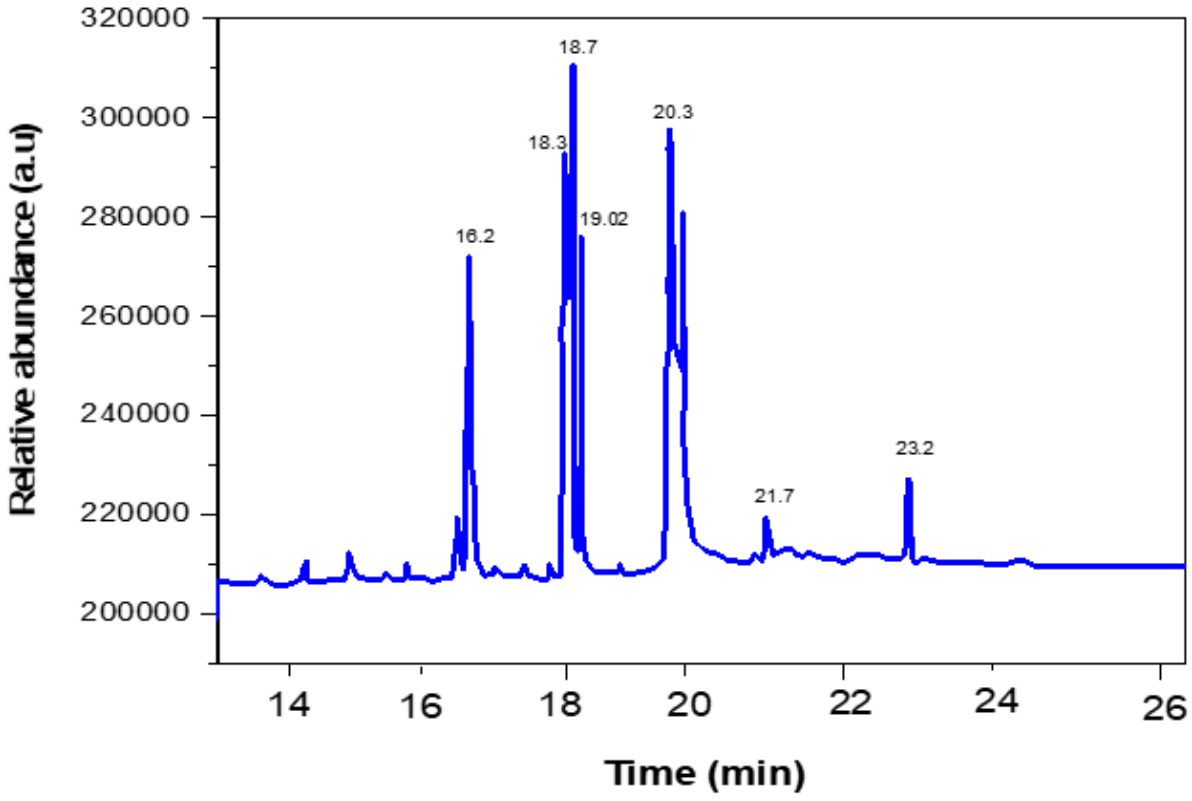

Figure 11

GC-MS curve of bio-fuel production from castor oil